Potential Predictability of Long-Term Drought and Pluvial Conditions in the U.S. Great Plains

SIEGFRIED D. SCHUBERT, MAX J. SUAREZ, PHILIP J. PEGION,* RANDAL D. KOSTER, AND JULIO T. BACMEISTER+

Global Modeling and Assimilation Office, Earth Sun Exploration Division, NASA GSFC, Greenbelt, Maryland

(Manuscript received 23 October 2006, in final form 19 June 2007)

ABSTRACT

This study examines the predictability of seasonal mean Great Plains precipitation using an ensemble of century-long atmospheric general circulation model (AGCM) simulations forced with observed sea surface temperatures (SSTs). The results show that the predictability (intraensemble spread) of the precipitation response to SST forcing varies on interannual and longer time scales. In particular, this study finds that pluvial conditions are more predictable (have less intraensemble spread) than drought conditions. This rather unexpected result is examined in the context of the physical mechanisms that impact precipitation in the Great Plains. These mechanisms include El Niño–Southern Oscillation's impact on the planetary waves and hence the Pacific storm track (primarily during the cold season), the role of Atlantic SSTs in forcing changes in the Bermuda high and low-level moisture flux into the continent (primarily during the warm season), and soil moisture feedbacks (primarily during the warm season). It is found that the changes in predictability are primarily driven by changes in the strength of the land–atmosphere coupling, such that under dry conditions a given change in soil moisture produces a larger change in evaporation and hence precipitation than the same change in soil moisture would produce under wet soil conditions. The above changes in predictability are associated with a negatively skewed distribution in the seasonal mean precipitation during the warm season—a result that is not inconsistent with the observations.

1. Introduction

The U.S. Great Plains experienced large fluctuations in precipitation during the last century. The 1930s and 1950s were, for example, characterized by severe drought conditions, while the early 1940s and 1990s saw relatively wetter conditions. The processes that contribute to such long-term (interannual to decadal) pluvial or drought conditions in the Great Plains have not been well established. A number of observational studies have linked summer precipitation in the Great Plains to changes in sea surface temperatures (SSTs). Trenberth and Guillemot (1996) linked tropical Pacific SST and convection anomalies associated with El Niño–Southern Oscillation (ENSO) to the 1988 drought and 1993 floods in the central United States. Ting and Wang (1997) found that decadal changes in U.S. summer precipitation are associated with SST anomalies in the North Pacific Ocean. Livezey and Smith (1999) found decadal covariability between U.S. surface temperature and a pan-Pacific SST pattern that encompasses the tropics and extratropics. Barlow et al. (2001) showed that there are three modes of SST variability related to long-term drought in the United States: an ENSO mode, a decadal pan-Pacific mode, and a North Pacific mode.

Recent studies employing long simulations with atmospheric general circulation models (AGCMs) forced with observed SSTs (e.g., Hoerling and Kumar 2003; Schubert et al. 2004a,b; Seager et al. 2005) also suggest that changes in SSTs play an important role in forcing the precipitation changes in the middle latitudes and particularly in the Great Plains. These studies point to

* Additional affiliation: Science Applications International Corporation, Beltsville, Maryland.

+ Additional affiliation: Goddard Earth Sciences and Technology Center, University of Maryland, Baltimore County, Baltimore, Maryland.

Corresponding author address: Siegfried D. Schubert, Global Modeling and Assimilation Office, Earth Sun Exploration Division, NASA GSFC, Greenbelt, MD 20771.
E-mail: siegfried.d.schubert@nasa.gov

DOI: 10.1175/2007JCLI1741.1

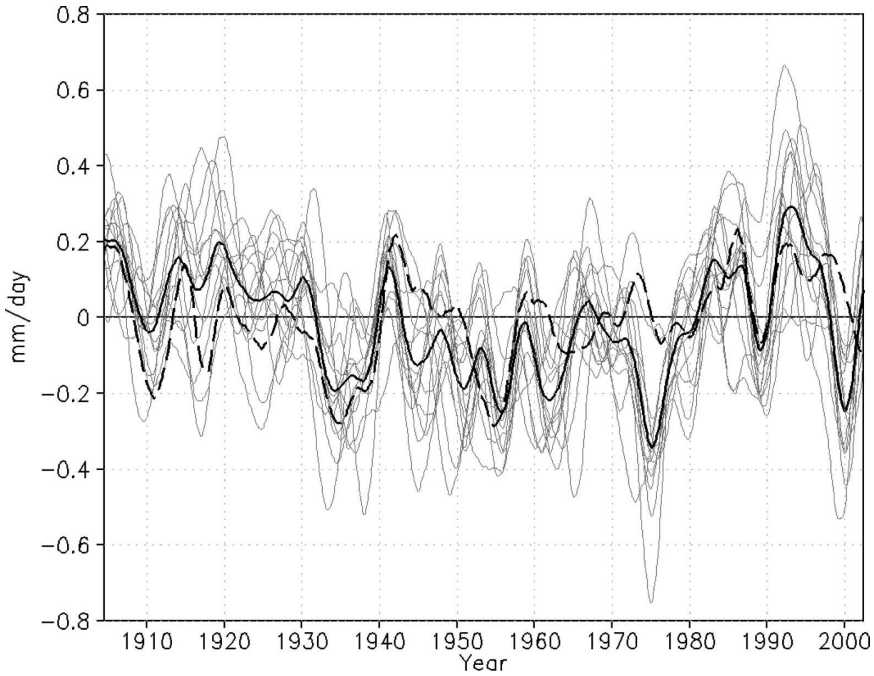

FIG. 1. Time series of precipitation anomalies (mm day^{-1}) averaged over the U.S. Great Plains (30°–50°N, 95°–105°W). A filter is applied to remove time scales shorter than about 6 yr. The 14 black curves are the individual ensemble members of the C20C runs produced with the NSIPP-1 model forced by observed SST and fixed CO_2. The heavy solid curve is the ensemble mean. The heavy dashed curve is from station observations. From Schubert et al. (2004b).

a number of physical mechanisms linking the changes in the tropical SSTs to changes in precipitation over North America. In particular, Seager et al. (2005) found that tropical Pacific SST anomalies are the primary cause of persistent droughts and wet conditions over western North America, and that this occurs as the result of SST-forced changes in the subtropical jets, transient eddies, and the eddy-driven mean meridional circulation. Schubert et al. (2004b) found that during the 1930s, tropical Atlantic SST anomalies also played an important role: the tropical Pacific SST anomalies forced changes in the planetary-scale waves and Pacific storm tracks (primarily during the winter and spring), while the tropical Atlantic/Caribbean SST anomalies forced changes in the Bermuda high and the associated low-level moisture flux into the continent (primarily during the summer and fall). In addition, land–atmosphere feedbacks acted to magnify the initial precipitation response to the SST.

The importance of land moisture conditions in the generation of rainfall anomalies is supported by a number of observational studies (e.g., Namias 1991; Bell and Janowiak 1995; Findell and Eltahir 1997; Koster et al. 2003). Koster et al. (2000) underscore the unique aspects of the Great Plains region that make rainfall in the region particularly sensitive to changes in soil moisture. Unambiguously quantifying the strength of soil moisture feedback on precipitation using observations alone, however, is difficult, if not impossible, and while the strength can be quantified precisely in AGCMs, these models (including the one used for this study) often seem to overestimate it (Koster et al. 2003; Ruiz-Barradas and Nigam 2005).

While the above model results show that there are SST-forced changes (including the modifying impact of land–atmosphere feedbacks) in the ensemble mean precipitation, we consider here the question of whether there are also changes in the intraensemble spread or predictability of the precipitation. Our study is motivated by the results in Fig. 1 (from Schubert et al. 2004b), showing the time history of Great Plains precipitation from an ensemble of National Aeronautics and Space Administration's (NASA) Seasonal-to-Interannual Prediction Project (NSIPP-1) AGCM simulations forced with twentieth-century observed SSTs. The figure shows what appear to be periods with reduced and enhanced spread among the ensemble members. For example, the 1930s drought has consid-

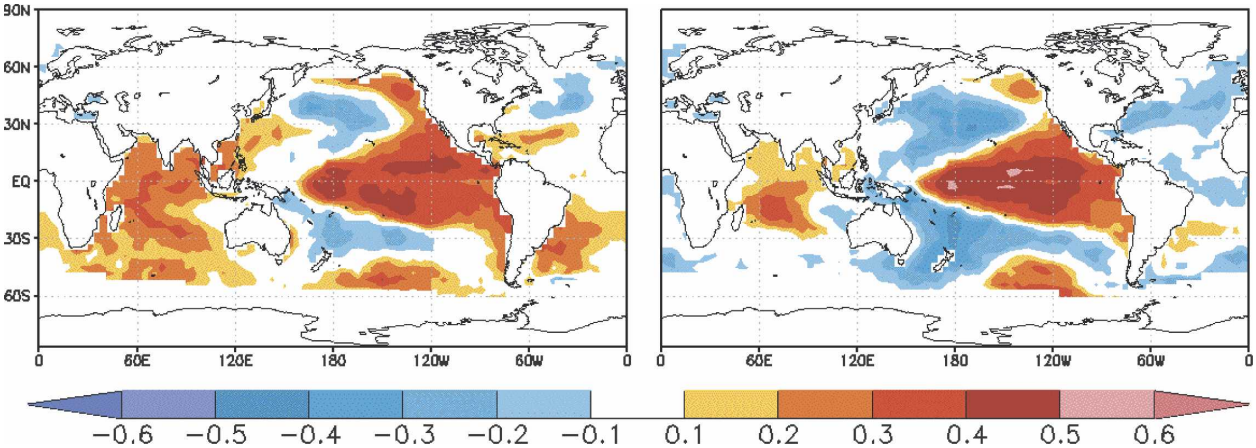

FIG. 2. Correlations between annual mean (left) observed (1901–2004) and (right) simulated (1902–2004) Great Plains precipitation and annual mean SST. For the simulations, the values are the average of 14 correlations produced for each ensemble member.

erable spread among the ensemble members, while the early 1940s (marking the end of the drought) shows less intraensemble spread.

We begin in section 2 by describing the model and the simulations. The results are presented in sections 3 and 4. Section 5 describes the physical mechanism responsible for the changes in predictability. The discussion and conclusions are given in section 6.

2. The AGCM simulations

Our study is based on a number of century-long simulations carried out with the NSIPP-1 atmospheric general circulation model run at a horizontal resolution of 3° latitude by 3.75° longitude and 34 unequally spaced σ layers with high resolution (<200 m) in the lower 2 km of the atmosphere. The dynamical core of the model is described in Suarez and Takacs (1995). The boundary layer scheme is a simple K-scheme, which calculates turbulent diffusivities for heat and momentum based on Monin–Obukhov similarity theory (Louis et al. 1982). The AGCM uses the relaxed Arakawa–Schubert (RAS) scheme to parameterize convection (Moorthi and Suarez 1992). The parameterization of solar and infrared radiative heating is described in Chou and Suarez (1994, 2000). The mosaic model (Koster and Suarez 1996) is used to represent land processes. Vegetation is prescribed with a climatological seasonal cycle. Details of the NSIPP-1 model formulation and its climate are described in Bacmeister et al. (2000). The seasonal predictability of the model is described in Pegion et al. (2000) for boreal winter and in Schubert et al. (2002) for boreal summer.

The model simulations used here are the same as those analyzed by Schubert et al. (2004b) and consist of an ensemble of fourteen 100-yr (1902–2001) runs forced by observed monthly SSTs (Rayner et al. 2002). The runs differ only in their initial atmospheric conditions. As such, the degree of similarity in the runs (the "signal") provides us with an assessment of the predictable component of the Great Plains climate variations, while the disagreement among the runs (the "noise") provides us with an estimate of the unpredictable component of the climate variability. Another set of eight simulations were performed that are identical to the original 14 runs, except that they include estimates of the time-varying CO_2 (the original set had a fixed modern value of CO_2). Since we found no significant impact on the precipitation in the Great Plains from the effects of the CO_2 changes on the atmospheric radiative heating rates (this is of course separate from the impact of CO_2 that would already be included in the SST forcing), these runs were included in our calculations. All together, these 22 runs were carried out as part of the Climate of the Twentieth Century Project (Folland et al. 2002) and are referred to here as the C20C runs.

The model results are compared with a Global Historical Climatology Network (GHCN) 5° latitude–longitude gridded station precipitation dataset available for the period 1900–2001 (Vose et al. 1992).

3. Results from the C20C runs

Our previous work (Schubert et al. 2004a,b) showed that the NSIPP-1 model does a credible job of reproducing the observed link between low-frequency changes in Great Plains precipitation and SSTs. Figure 2, for example, compares the correlations between the observed precipitation and SST (left panel) with the correlation between the simulated precipitation and

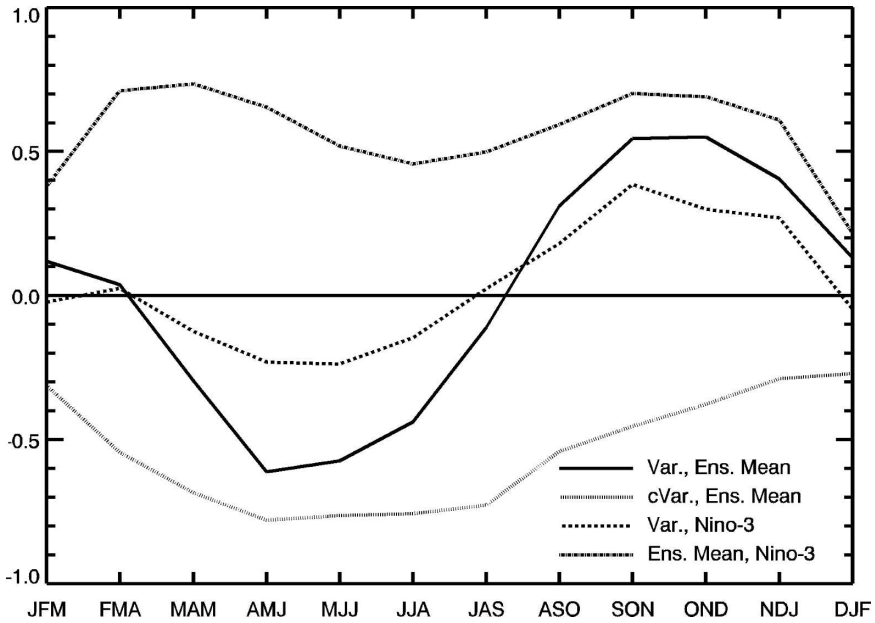

FIG. 3. Various correlations of interannual variability of seasonal mean Great Plains precipitation. The solid line shows the correlations between the intraensemble variance and ensemble mean. The dotted line shows the correlations between the coefficient of variation and ensemble mean. The dashed line shows the correlations between the intraensemble variance and Niño-3 SST, and the dot–dash line shows the correlations between the ensemble mean and Niño-3 SST.

SST averaged over all ensemble members. The results show that the model reproduces the relatively strong correlations with the Pacific SSTs (in particular the ENSO-like pattern), as well as the positive correlations over the Indian Ocean (though these are not as extensive as those found in the observations). There are some differences in the tropical Atlantic, with the simulation showing positive correlations while the observations show weak or slightly negative values. It is unclear whether the positive correlations indicate an incorrectly modeled physical connection between the tropical Atlantic and Great Plains precipitation, or whether they simply reflect a correlation between the SSTs in the Pacific and Atlantic Oceans that is not picked up by the more limited set of observations. In any event these correlations are rather weak, and the overall results give us confidence that the model is performing well and that we can look further into the higher-order (second moment) statistics involving the relationship between the SST and Great Plains precipitation.

a. Intraensemble spread and the ensemble mean

We focus here on the spread among the ensemble members (the so-called intraensemble spread) as a measure of predictability or robustness of the response to the SST and its relationship with the ensemble mean. It is important to note that we are not addressing the full predictability problem, which must of course also include the uncertainties that occur in predicting the SSTs.

Figure 3 summarizes the correlations between the ensemble mean and intraensemble variance. There is a rather remarkable annual cycle in the correlations, with negative correlations occurring in spring and summer and positive correlations occurring in fall and winter. The largest negative values occur in late spring and summer, while the largest positive values occur during the fall. The correlations between the ensemble mean and the square of the coefficient of variation (defined as the intraensemble standard deviation divided by the ensemble mean) show all negative correlations, consistent with what one might expect from, for example, a gamma distribution. The positive correlations between the ensemble mean and variance simply reflect the fact that the precipitation statistics tend to have a positive skewness (large variances are associated with large values), and normalizing the variance by the square of the mean removes that dependence (it in fact makes the correlations negative). The more interesting results to explain are the negative correlations between the ensemble mean and variance during the spring and summer. This apparently reflects a physical process that

produces negative skewness in the precipitation statistics. We see that the correlations between the intraensemble variance of the Great Plains precipitation and the Niño-3 index have an annual cycle that is very similar to that of the correlations between the intraensemble variance and the ensemble mean, reflecting the fact that the ensemble mean precipitation is to a large extent forced by the tropical Pacific SST. This connection is highlighted by the correlations between the ensemble mean and the Niño-3 index: these are positive throughout the year, with the strongest correlations occurring during the spring and fall seasons. We will discuss the seasonality of the skewness of the precipitation statistics further in section 5 (see, e.g., Fig. 11)

b. Composite fields

The negative correlation during the spring and summer (the rainy seasons) suggests that pluvial conditions are more predictable than drought conditions in the Great Plains. In this section we look into the nature of the physical mechanisms that might produce the negative correlations between the intraensemble variance and the ensemble mean. We begin by examining the meteorology associated with those years that have either very large or very small intraensemble variance. We first composite the SST anomalies based on the values of the coefficient of variation of Great Plains precipitation. In particular, we form one SST composite by averaging together those years with coefficient of variation values greater than one standard deviation, and another SST composite by averaging together those years with coefficient of variation values less than negative one standard deviation. Figure 4 shows the composites for each season. In view of the strong negative correlations during April–June (AMJ; Fig. 3), we focus on that "season" instead of the usual March–May (MAM) season. All but December–February (DJF) show a coherent global signal associated with the changes in intraensemble spread in the Great Plains precipitation. These seasons [AMJ, June–August (JJA), September–November (SON)] show what appear to be La Niña– (El Niño) like SST anomalies characterized by negative (positive) anomalies in the tropical Pacific surrounded by positive (negative) anomalies to the north and south. The La Niña anomalies occur for the large variability cases, while the small variability cases are associated with the El Niño anomalies. On the other hand, during DJF the SST composites are weaker, suggesting that any differences in the precipitation variability in the Great Plains are not linked to SST changes during that season.

The above results link La Niña or cold tropical Pacific SST to both a reduction (in the mean) and greater variability in the Great Plains precipitation, while El Niño or warm tropical Pacific SSTs are associated with both an enhancement (in the mean) and less variability in the Great Plains precipitation for all but the winter season, consistent with the correlations shown in Fig. 3. The basic question then is whether this apparent relationship between the SST anomalies and variability in the Great Plains precipitation is the result of direct SST-forced changes in the variability of the atmospheric circulation, or whether it is tied to differences in local land–atmosphere processes that are an indirect consequence of the SST anomalies through its impact on the mean land surface conditions (dry or wet). Since the negative correlation between the mean and variance is strongest during AMJ, we will in the following focus on that season with the goal of understanding the physical mechanisms responsible for such a relationship.

We next look at composites of the global 200-mb height field during AMJ (Fig. 5). The results show the expected ENSO-like responses characterized by a wavelike response to the tropical Pacific. The La Niña anomalies consist of positive height anomalies in the middle latitudes that would tend to suppress storm development in the North Pacific and/or divert the storm tracks away from the continental United States. The El Niño anomalies, in contrast, consist of negative height anomalies in the middle latitudes that would tend to enhance storm development in the North Pacific and/or facilitate the storms entering the continental United States. Schubert et al. (2001) show that a strong La Niña tends to have greater intraensemble variability in the circulation over the North Pacific and North America, while a strong El Niño has less variability. The differences in the variability are the result of differences in the stability of the wintertime East Asian jet. Such a difference in the variability of the large-scale winter (and perhaps spring) circulation could potentially lead to the negative correlations between the mean and variance of the precipitation found here.

The top panel of Fig. 6 shows the differences in the 200-mb height variability between years with large and those with small AMJ Great Plains precipitation variability. The results show that, while there is increased variability over Canada and the northeastern United States, the variability over the western United States extending into the Great Plains is in fact reduced, so it is unlikely that changes in large-scale variability are playing a direct role. While we did not find a strong negative correlation between the mean precipitation and its variance for winter (DJF), it may be that the

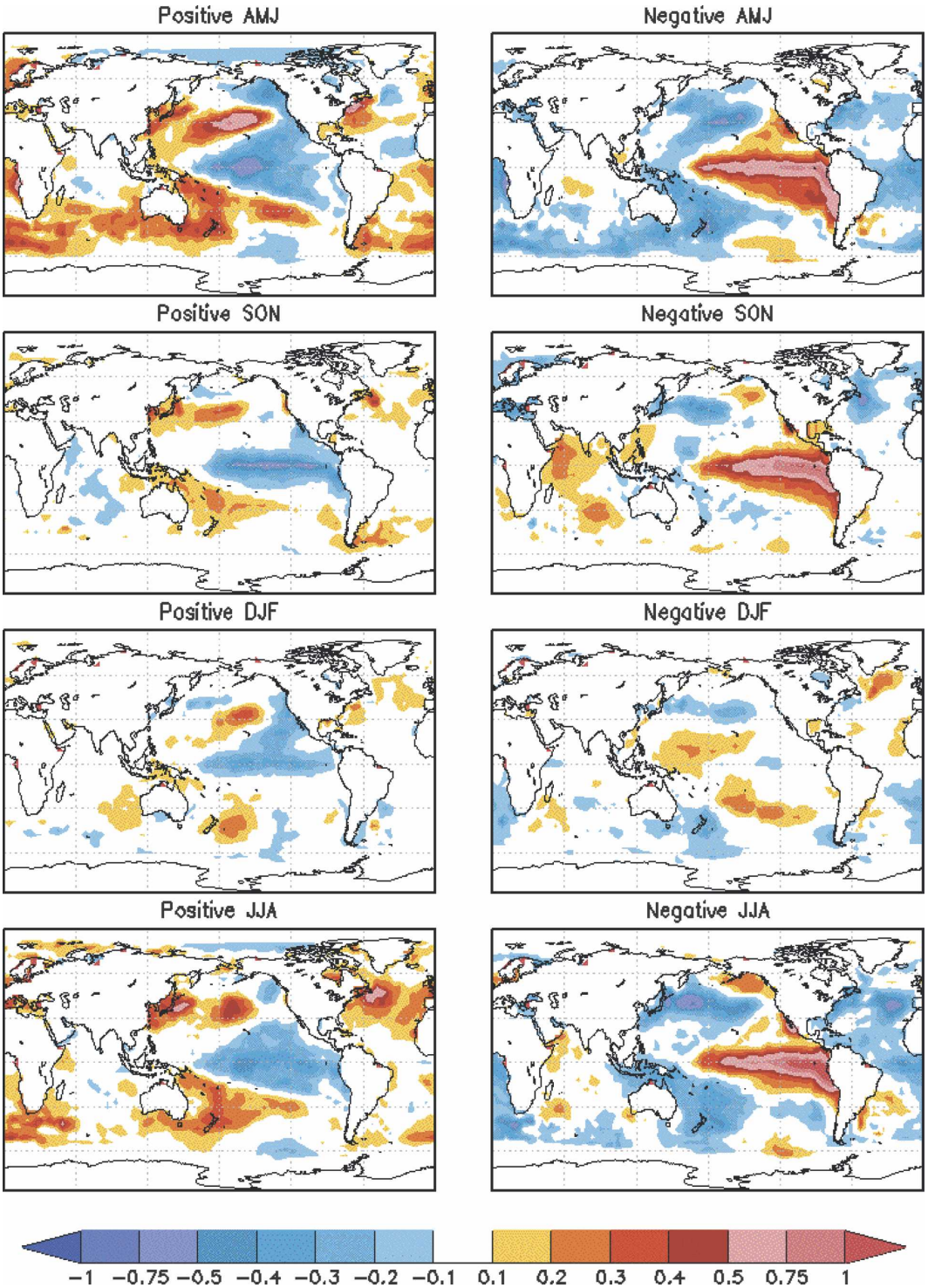

FIG. 4. SST anomaly (°C) composites based on the years with (left) the largest (>1 std dev) and (right) smallest (<−1 std dev) values of the coefficient of variation of Great Plains precipitation (1902–2004).

relationship comes primarily through the impact on the spring precipitation variability of the antecedent (winter) variability. To see if that is the case, we show in the bottom panel of Fig. 6 the differences in the January–March (JFM) 200-mb height variability between years with large and those with small AMJ Great Plains precipitation variability. Here again, while there are increases over the North Pacific, Alaska, and the Pacific

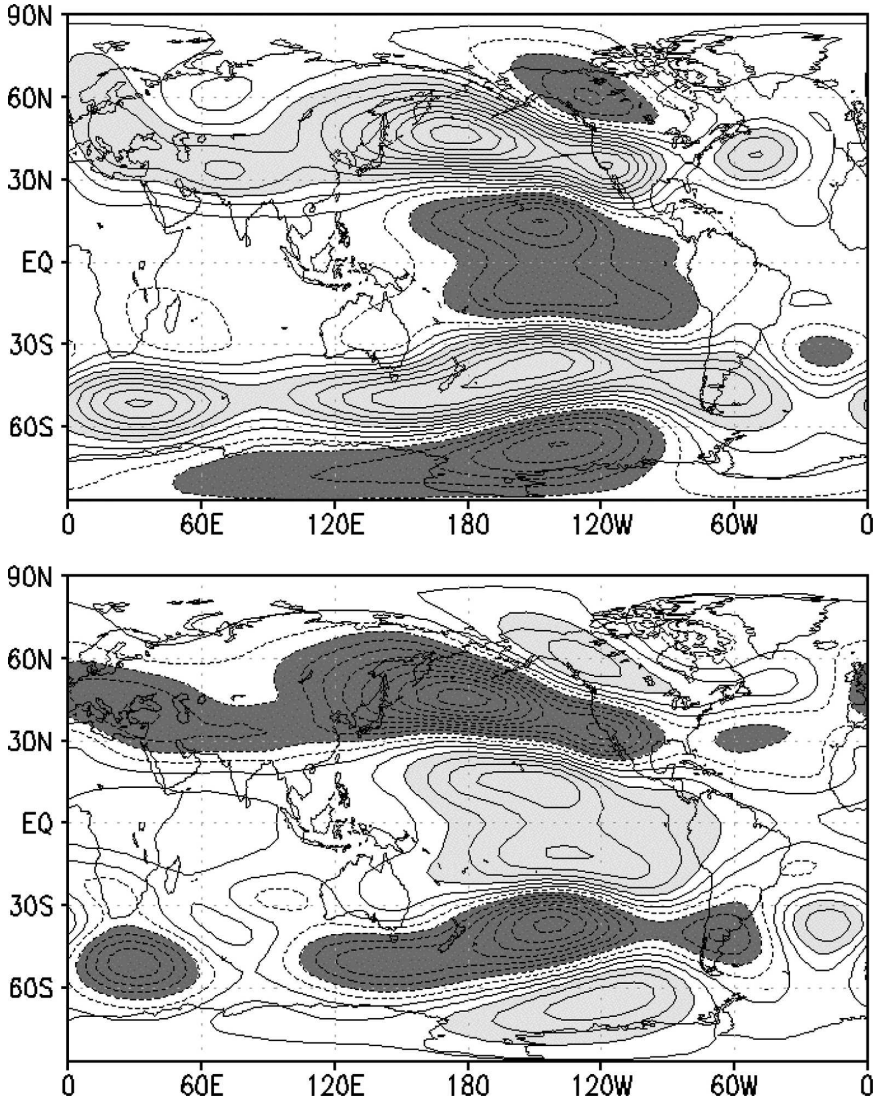

FIG. 5. The 200-mb height anomaly (AMJ) composites based on the years with the (top) largest (>1 std dev) and (bottom) smallest (<−1 std dev) values of the coefficient of variation of Great Plains precipitation (1902–2004). The contour interval is 4 m. Dashed contours represent negative values. Light shading for values greater than 8 m; dark shading for values less than −8 m.

Northwest, we do not see any other significant impact over the United States. We find similar results for the changes in the JFM precipitation variability (not shown), which show some reduction in variability along the West Coast and the Southeast.

The above results suggest that we must look to local processes for understanding the physical mechanisms producing the changes in variability. This includes changes in land–atmosphere interactions and possibly changes in the variability of the low-level winds associated with the low-level jet (LLJ). Figure 7 shows the differences in the precipitation, evaporation, and 925-mb wind variability between years with large and those with small AMJ Great Plains precipitation variability. The increase in precipitation variability (top panel) over the Great Plains is not surprising since that simply reflects how the composites were developed. It is interesting that there is also a very clear signal in the evaporation, with an increase in evaporation that extends over the same domain as the increase in precipitation variability. The third panel shows that there is also an increase in the low-level wind variability, though that is very small and so it is unlikely to impact the results.

In view of the above results we next focus our atten-

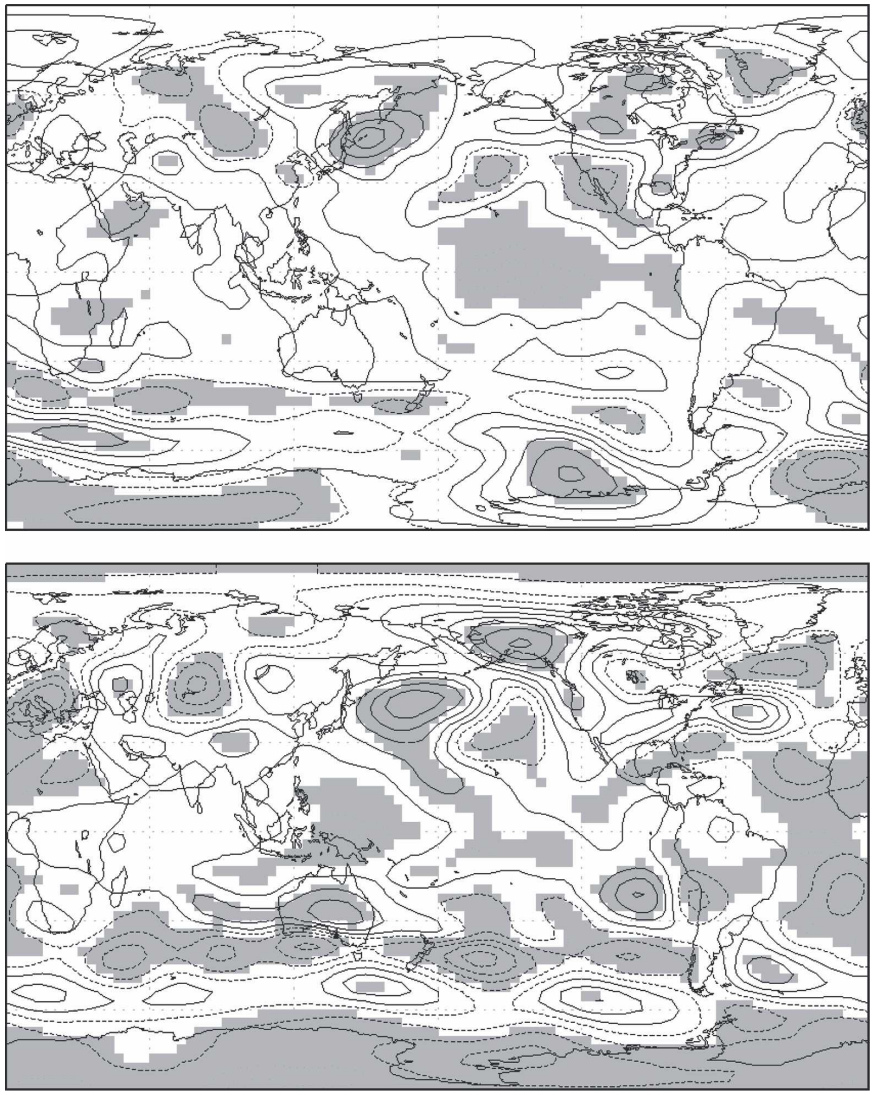

FIG. 6. Differences in the (top) AMJ and (bottom) JFM intraensemble std dev (σ) of the 200-mb height field computed as the mean σ of the years with the largest (>1 std dev) minus the mean σ of the years with the smallest (<−1 std dev) values of the coefficient of variation of AMJ Great Plains precipitation (1902–2004). The contour interval is 2 m. Shading indicates differences that are significant at the 20% level of an F test.

tion on the land surface processes operating during AMJ.

4. Idealized SST experiments

In this section we attempt to reproduce the changes in precipitation variability during AMJ in a set of controlled AGCM simulations in which we force the model with the two polarities of the AMJ composite SST pattern shown in the top panels of Fig. 4. In one polarity (left top panel, negative anomalies in the tropical Pacific) the SST anomalies are associated with enhanced intraensemble Great Plains precipitation variability, while in the other polarity (right top panel, positive anomalies in the tropical Pacific) the SST anomalies are associated with reduced intraensemble Great Plains precipitation variability.

We carry out 100 simulations (1 March–30 June) for each SST anomaly pattern. The 100 runs for each SST pattern differ only in the initial (1 March) atmosphere and land initial conditions: these are taken at random from existing century-long simulations. Both sets of runs are then repeated but with the soil moisture feedbacks disabled in the AGCM. In these runs we fix the

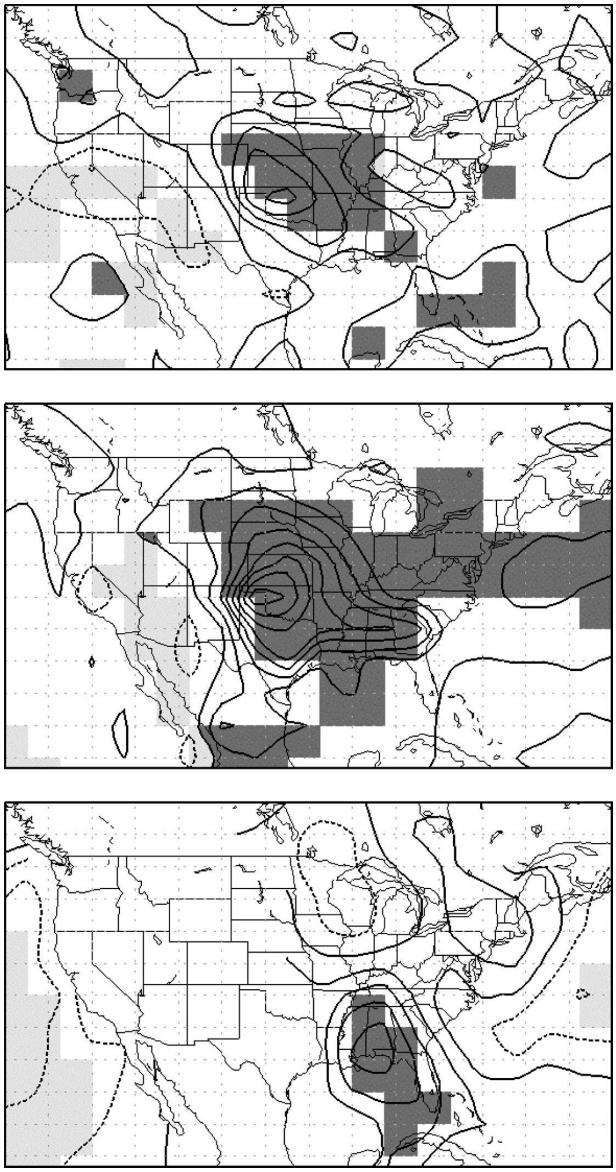

FIG. 7. Difference in the AMJ intraensemble standard deviation (σ) of selected quantities computed as the mean σ of the years with the largest (>1 std dev) minus the mean σ of the years with the smallest (<−1 std dev) values of the coefficient of variation of AMJ Great Plains precipitation (1902–2004). (top) Precipitation (contour interval is 0.1 mm day^{-1}), (middle) evaporation (contour interval is 2 W m^{-2}), and (bottom) 925-mb v-wind component (contour interval is 0.05 m s^{-1}). Shading indicates significance as in Fig. 6.

land surface model's evaporation efficiency or "β" (the ratio of the evaporation to the potential evaporation) to its seasonal climatology, as described in Koster et al. (2000). The potential evaporation is the maximum rate at which the atmosphere can receive water (as controlled by near-surface humidity gradients, wind speed, etc.).

The impact of the two SST patterns on U.S. precipitation is shown in Fig. 8, plotted as the difference between the two sets of runs. The top panels show the impact on the ensemble seasonal mean and the bottom panels show the impact on the variance of the seasonal means. The right panels are for the cases in which the soil moisture feedbacks are disabled. We see the expected precipitation deficit in Great Plains precipitation (upper left panel) consistent with our previous studies on the impact of the tropical Pacific SSTs (e.g., Schubert et al. 2004b). The precipitation deficit extends to the Southeast, the West, and into northern Mexico. The variance difference (lower left panel) is positive over much of the Great Plains, especially over the southern states. Differences are shaded where they are significant at the 5% level based on an F test. Significant differences also occur over the Caribbean Sea and the Pacific Northwest. The right panels show that without soil moisture feedback the mean precipitation deficit is reduced (consistent with, e.g., Schubert et al. 2004b), and the enhanced precipitation variability in the Great Plains is completely absent. We note that the other regions of enhanced variability over the Caribbean Sea and the Pacific Northwest remain, indicating that the variability in those regions is not associated with land surface processes.

Figure 9 is the same as in Fig. 8 but for the evaporation. Here (top left panel) we see a reduction in evaporation over the same regions that we saw a reduction in precipitation, with the largest reductions occurring over the southern Great Plains. Enhanced evaporation occurs off the East Coast and in the Gulf of Mexico. Much of the southern Great Plains and the Southeast shows enhanced evaporation variability. Comparisons with the geographical distribution of the change in precipitation variability (Fig. 8) suggest a strong link between the changes in variability of these two quantities. The impact of disabling the soil moisture feedbacks is to eliminate most of the changes over land, including the evaporation deficits (top right panel) and enhanced variability over the Great Plains (lower right panel).

5. A physical mechanism

The above results show that soil moisture feedbacks are necessary for producing the changes in precipitation variability in the Great Plains during AMJ, and that the change appears to be strongly linked to changes in the variability of evaporation. In the following, we outline the physical processes by which dry conditions (precipitation deficits) can be associated with enhanced precipitation variability, while wet conditions (precipitation surplus) can be associated with reduced precipitation variability in the Great Plains.

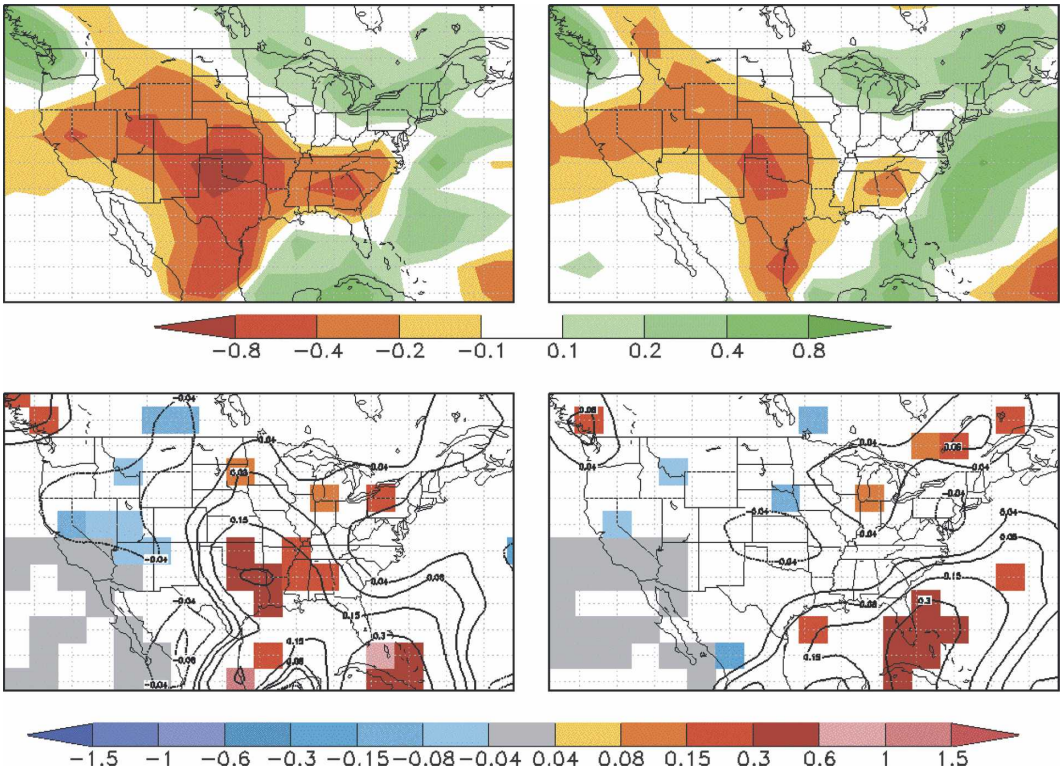

FIG. 8. Difference in the (top) mean (μ) and (bottom) variance (σ^2) of the AMJ precipitation computed from the idealized SST runs. The differences are computed as the variance of 100 April through June simulations forced with the SST field shown in the top left panel of Fig. 4 minus the variance of 100 April through June simulations forced with the SST field shown in the top right panel of Fig. 4. The right panels are for the runs in which soil moisture feedbacks are disabled (see text for details). The runs are initialized with arbitrary 1 Mar atmosphere and land states from long Atmospheric Model Intercomparison Project (AMIP) style simulations. Units are mm day^{-1} in the top panels and (mm day^{-1})^2 in the bottom panels. Shading indicates significance at the 5% level based on an F test.

Figure 10 shows a scatterplot relating near-surface soil moisture to the evaporation divided by net radiation or "evaporative fraction" (e.g., Shuttleworth 1991). The use of evaporative fraction instead of evaporation for this plot is motivated by the following: in a simplified sense, evaporation is controlled by two things, the dryness of the soil and the incident energy on the surface. If we were to plot instead evaporation against soil moisture, we would get a lot of scatter, because some points on the plot would be high due to high net radiative energy, and some would be low due to low net radiative energy. By "normalizing" the evaporation by the available energy (the net radiation) before producing the scatterplot, we hone in on the relevant relationship with soil moisture, the relationship that links variability in the land moisture state to variability in evaporation and thus to droughts and pluvials.

The crosses in Fig. 10 are the AMJ mean values from a large number of simulations with the NSIPP-1 AGCM, including the 22 C20C runs and several 100+ yr simulations forced with climatological SSTs. The scatter of points (the black line is a cubic fit) shows that the slope of the apparent relationship is relatively steep for small soil moisture values and decreases as we move toward wetter soil conditions. Such a shape is not unexpected. The curvature stems from the fact that when the soil is relatively dry, evaporation is limited by the ability of the soil to provide water to the atmosphere, whereas when the soil is very wet, it can provide water easily and evaporation is limited instead by the atmosphere's ability to accept the water (e.g., Budyko 1974; Manabe 1969; Eagleson 1978). Evaporative fraction is therefore sensitive to soil moisture variations when soil moisture is low and is relatively insensitive to such variations when soil moisture is high. The curvature shown in the figure reflects the transition between these two hydroclimatological regimes.

Because of this curvature, a given change in soil moisture has a larger impact on the evaporative fraction in the dry regime than it does in the wet regime.

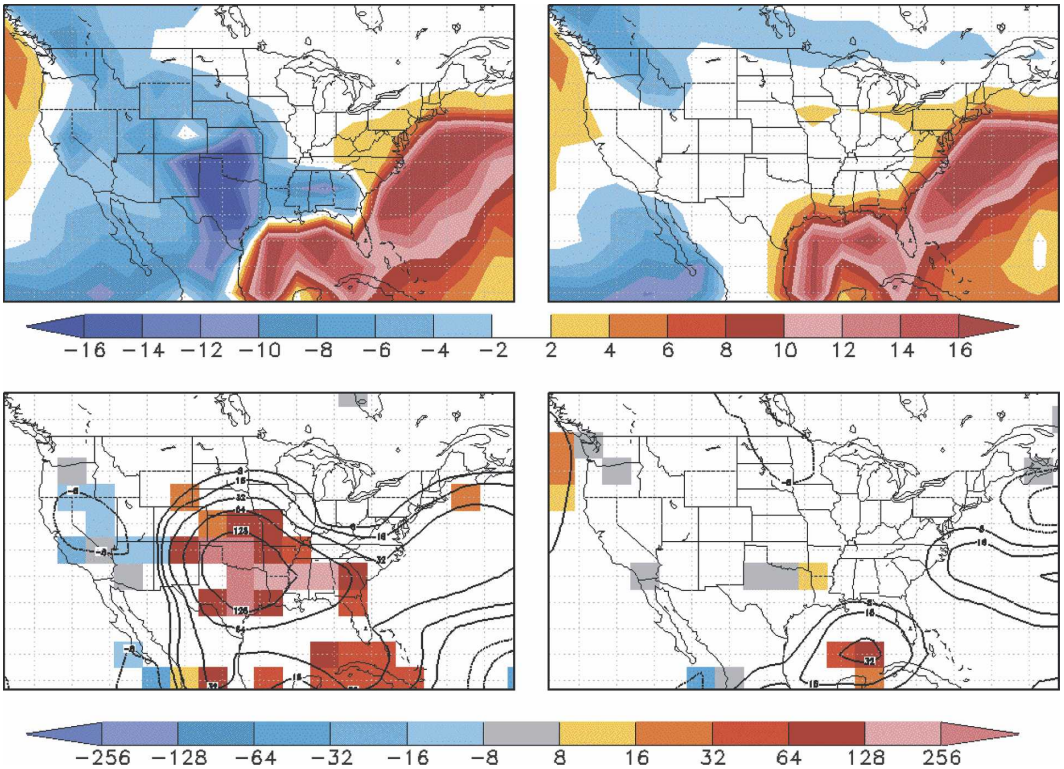

FIG. 9. Same as Fig. 8, but for evaporation. Units are W m^{-2} in the top panels and $(W\ m^{-2})^2$ in the bottom panels.

This is illustrated clearly by our two sets of simulations with the idealized SST. The red dots in Fig. 10 show the 100 AMJ values for the cases forced with negative SST anomalies in the tropical Pacific (left top panel of Fig. 4), while the blue dots are for the cases forced with positive SST anomalies in the tropical Pacific (right top panel of Fig. 4). The results show how the dryer conditions for the red dots put them on a steeper part of the curve so that the change in evaporative fraction (as represented by the separation of the horizontal lines) is considerably larger than that for the blue dots with essentially the same change in soil moisture (as represented by the separation of the vertical lines, set to twice the standard deviation of the soil moisture values). We note that both sets of runs have basically the same soil moisture variability.

The above results link changes in soil moisture to changes in the evaporative fraction that in turn lead to changes in precipitation. Since the link between soil moisture and evaporative fraction is stronger for dryer soil values (at least up to a point, since if the soil gets too dry it presumably will have less variability since it is bounded from below by zero), we argue that the dryer soils associated with drought conditions tend to promote greater evaporation variability and thus greater precipitation variability than do the wetter soils associated with pluvial conditions. The response of precipitation to soil moisture variations is particularly strong in the Great Plains in this model (Koster et al. 2000), as it is in several models (Koster et al. 2006a).

Of course, a key question is whether the same mechanism operates in nature. Our ability to identify signatures of the mechanism in the observational data is hampered by two things. First, the AGCM used here is known to exaggerate the strength of land–atmosphere coupling in the Great Plains (Koster et al. 2003), so that signatures present in the observational data are expected to be weaker (though still nonzero) than those implied by the model results. Second, and more importantly, the observational data are limited. Nature provides us with only a single "realization," and thus observations-based "intra-ensemble variances" for drought and pluvial conditions cannot be computed. While a key consequence of the negative correlation between the mean and variance is a negative skewness for the precipitation, and while this is a quantity that can be directly computed, the observational data span only about a 100 yr and have large uncertainties (particularly in the early years), diminishing our ability to determine reliable values.

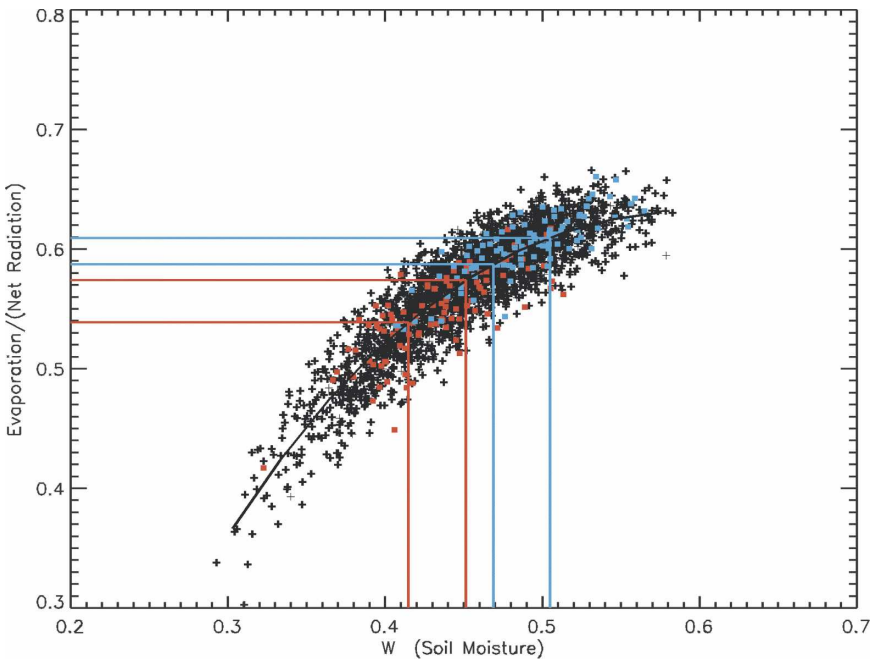

FIG. 10. The plus symbols show the scatter of soil moisture vs the ratio of evaporation/net radiation, that is, evaporative fraction, for AMJ from the 22 C20C runs (1902–2004), several 100+ yr runs with climatological (1902–2004 average) SST, and the two 100-member AMJ idealized SST ensemble runs (the red dots highlight the results from the 100 AMJ simulations forced with the SST pattern shown in the top left panel of Fig. 4, while the blue dots highlight the results from the 100 AMJ simulations forced with the SST pattern shown in the top right panel of Fig. 4). The black curve is a cubic fit to the results from all the runs. The vertical lines show 1 std dev in the red (blue) soil moisture values centered on the mean of the red (blue) value. The horizontal lines show the corresponding change in the evaporative fraction (0.035 for red and 0.022 for the blue) associated with the 1 std dev change in the soil wetness (0.037 for red and 0.036 for blue).

We note, however, that an earlier study of historical observational temperature data (Koster et al. 2006b) provides evidence that the shape of the curve in Fig. 10 does indeed affect the statistics of real-world evaporation in a manner consistent with the proposed mechanism. In addition, despite the aforementioned difficulties with the historical record, the observational precipitation data, when averaged over the Great Plains, do show a tendency for negative skewness during JJA (Fig. 11, top left panel), with a value of −0.08 computed from the data directly and a value of −0.16 computed from the fitted Weibull distribution (compared to −0.43 for the model, top right panel). The observations-based skewness, however, is not negative during AMJ [though it is slightly negative during May–July (MJJ)], the season analyzed above for the AGCM. This may be because, as mentioned above, land–atmosphere feedback in this AGCM is overestimated. In the AGCM, feedback during AMJ is reduced relative to that in JJA but is still significant, and the curvature effect (Fig. 10) is particularly strong. The net result is a strong negative correlation between precipitation mean and variance. In the real world, on the other hand, land–atmosphere feedback during the colder AMJ season may simply be too small for the curvature to have an impact. Most of the cold season, in fact, does exhibit a positive skewness in both the observed and simulated precipitation distribution. Figure 11 (bottom panels) shows, for example, the histograms for October–December when both the observations and the model show a clear positive skewness.

Despite the exaggeration inferred for the simulation, these results provide some insight into a mechanism that must be considered when evaluating the predictability of drought and pluvial conditions in the Great Plains, and potentially in other regions of the world where there is substantial coupling between the land and atmosphere (Koster et al. 2004).

6. Discussion and conclusions

This study examined the causes of the temporal changes in intraensemble variance of the seasonal mean

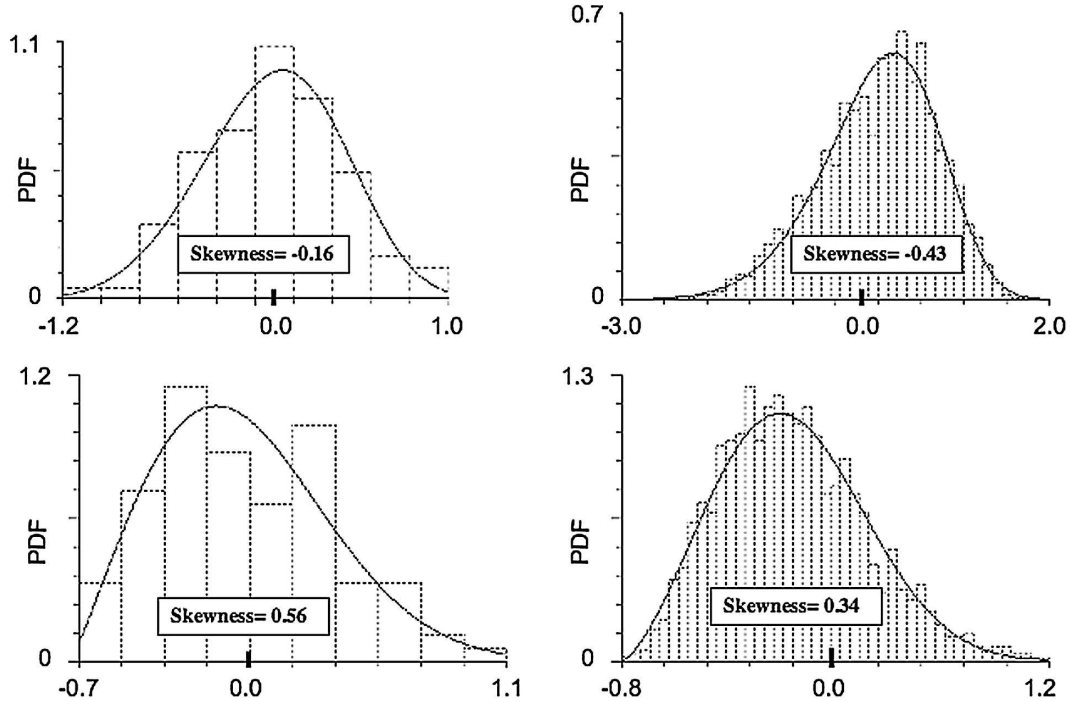

FIG. 11. Histograms of seasonal mean Great Plains (30°–50°N, 95°–105°W) precipitation (mm day^{-1}) for (top) JJA and (bottom) October–December (OND) with superimposed fits to the Weibull distribution. The left panels are for the observations (1901–2004), and the right panels are for the model simulations (22 ensemble members, 1902–2004). Skewness values shown are computed from the fitted distributions. For comparison, the corresponding skewness values computed using (A1) are for the observations (JJA: −0.085, OND: 0.42) and for the model (JJA: −0.42, OND: 0.47).

Great Plains precipitation simulated by the NSIPP-1 AGCM when forced with the twentieth-century observed SSTs. A key finding is that the correlation between the ensemble mean and the intraensemble variance of the seasonal mean precipitation has negative correlations during the warm season. The negative correlations are unexpected for a quantity such as precipitation that tends to have a positively skewed distribution.

An analysis of the simulations suggested that the negative correlations are linked to differences in the local land–atmosphere interactions, and not to any differences in the large-scale atmospheric dynamics during dry and wet years. In particular, we showed how differences in the strength of the soil moisture feedbacks under changing soil conditions can lead to greater changes in evaporation (and therefore precipitation) for a given change in soil moisture when the soil is relatively dry. Whether this mechanism operates in nature depends on whether nature has a relationship between soil wetness and evaporation similar to that shown in Fig. 10. Our calculations of skewness from the observational data suggest that this may be the case, though the degree of negative skewness during the warm season is considerably less than that of the model simulations. In a related study, Koster et al. (2006b) examined the impact of the relationship in Fig. 10 on the higher moments of near-surface air temperature. The shape of the relationship was found to have profound impacts on the spatial distributions of the temperature moments in the model. These temperature signatures were also found (to a large degree) in the observational data, suggesting that the relationship in Fig. 10 is indeed operating in nature.

The above results have potentially important implications for predicting drought. They suggest, for example, that predictions of the demise of an existing drought might be more skillful than predictions of the onset of drought, assuming land moisture conditions at the beginning of the forecast period are unknown. It is interesting to note that a number of the major droughts of the twentieth century (e.g., the 1930s Dust Bowl drought) ended with a major El Niño event, and so predicting the demise of a drought will likely depend on our ability to predict both the El Niño event and the remote atmospheric–land response to the SSTs.

Acknowledgments. This work was supported by the NASA Energy and Water cycle Study (NEWS) pro-

gram, and the NASA Modeling and Analysis Program (MAP).

APPENDIX

Skewness Calculations

Skewness is a measure of the asymmetry of a probability density function and is defined as the ratio of the third moment to the third power of the standard deviation. We estimate the skewness of a quantity x for a sample of size n by

$$g_1 = \frac{n\sqrt{n-1}}{n-2}\left\{\frac{\sum_{i=1}^{n}(x_i-\overline{x})^3}{\left[\sum_{i=1}^{n}(x_i-\overline{x})^2\right]^{3/2}}\right\}. \qquad \text{(A1)}$$

As an additional estimate of skewness, we also first fit the data to the Weibull probability distribution—a distribution that is commonly used to fit hydrologic data (e.g., Jawitz 2004) and that appears to be a good fit to our seasonal mean simulated and observed precipitation data.

REFERENCES

Bacmeister, J., P. J. Pegion, S. D. Schubert, and M. J. Suarez, 2000: Atlas of seasonal means simulated by the NSIPP 1 atmospheric GCM. NASA Tech. Memo. 104606, Vol. 17, 190 pp. [Available from Goddard Space Flight Center, Greenbelt, MD 20771.]

Barlow, M., S. Nigam, and E. H. Berbery, 2001: ENSO, Pacific decadal variability, and U.S. summertime precipitation, drought, and streamflow. *J. Climate,* **14,** 2105–2128.

Bell, G. D., and J. E. Janowiak, 1995: Atmospheric circulation associated with the Midwest floods of 1993. *Bull. Amer. Meteor. Soc.,* **76,** 681–695.

Budyko, M. I., 1974: *Climate and Life*. Academic Press, 508 pp.

Chou, M.-D., and M. J. Suarez, 1994: An efficient thermal infrared radiation parameterization for use in general circulation models. NASA Tech. Memo. 104606, Vol. 3, 85 pp. [Available from Goddard Space Flight Center, Greenbelt, MD 20771.]

——, and ——, 2000: A solar radiation parameterization for atmospheric studies. NASA Tech. Memo. 104606, Vol. 11, 40 pp. [Available from Goddard Space Flight Center, Greenbelt, MD 20771.]

Eagleson, P. S., 1978: Climate soil and vegetation. 4. The expected value of annual evapotranspiration. *Water Resour. Res.,* **14,** 731–739.

Findell, K., and E. A. B. Eltahir, 1997: An analysis of the soil moisture–rainfall feedback based on direct observations from Illinois. *Water Resour. Res.,* **33,** 725–735.

Folland, C., J. Shukla, J. Kinter, and M. Rodwell, 2002: The Climate of the Twentieth Century Project. *CLIVAR Exchanges,* No. 7, International CLIVAR Project Office, Southampton, United Kingdom, 37–39.

Hoerling, M. P., and A. Kumar, 2003: The perfect ocean for drought. *Science,* **299,** 691–694.

Jawitz, J. W., 2004: Moments of truncated continuous univariate distributions. *Adv. Water Res.,* **27,** 269–281.

Koster, R. D., and M. J. Suarez, 1996: Energy and water balance calculations in the MOSAIC LSM. NASA Tech. Memo. 104606, Vol. 9, 194 pp. [Available from Goddard Space Flight Center, Greenbelt, MD 20771.]

——, ——, and M. Heiser, 2000: Variance and predictability of precipitation at seasonal-to-interannual timescales. *J. Hydrometeor.,* **1,** 26–46.

——, ——, R. W. Higgins, and H. Van den Dool, 2003: Observational evidence that soil moisture variations affect precipitation. *Geophys. Res. Lett.,* **30,** 1241, doi:10.1029/2002GL016571.

——, and Coauthors, 2004: Regions of strong coupling between soil moisture and precipitation. *Science,* **305,** 1138–1140.

——, and Coauthors, 2006a: GLACE: The Global Land–Atmosphere Coupling Experiment. Part I: Overview. *J. Hydrometeor.,* **7,** 590–610.

——, M. J. Suarez, and S. D. Schubert, 2006b: Distinct hydrological signatures in observed historical temperature fields. *J. Hydrometeor.,* **7,** 1061–1075.

Livezey, R., and T. Smith, 1999: Covariability of aspects of North American climate with global sea surface temperatures on interannual to interdecadal timescales. *J. Climate,* **12,** 289–302.

Louis, J., M. Tiedtke, and J. Geleyn, 1982: A short history of the PBL parameterization at ECMWF. *Proc. ECMWF Workshop on Planetary Boundary Layer Parameterization,* Reading, United Kingdom, ECMWF, 59–80.

Manabe, S., 1969: Climate and the ocean circulation. I. The atmospheric circulation and the hydrology of the earth's surface. *Mon. Wea. Rev.,* **97,** 739–774.

Moorthi, S., and M. J. Suarez, 1992: Relaxed Arakawa–Schubert: A parameterization of moist convection for general circulation models. *Mon. Wea. Rev.,* **120,** 978–1002.

Namias, J., 1991: Spring and summer 1988 drought over the contiguous United States—Causes and prediction. *J. Climate,* **4,** 54–65.

Pegion, P. J., S. D. Schubert, and M. J. Suarez, 2000: An assessment of the predictability of northern winter seasonal means with the NSIPP 1 AGCM. NASA Tech. Memo. 104606, Vol. 18, 107 pp. [Available from Goddard Space Flight Center, Greenbelt, MD 20771.]

Rayner, N. A., D. E. Parker, E. B. Horton, C. K. Folland, L. V. Alexander, D. P. Rowell, E. C. Kent, and A. Kaplan, 2002: Global analyses of sea surface temperature, sea ice, and night marine air temperature since the late nineteenth century. *J. Geophys. Res.,* **108,** 4407, doi:10.1029/2002JD002670.

Ruiz-Barradas, A., and S. Nigam, 2005: Warm season rainfall variability over the U.S. Great Plains in observations, NCEP and ERA-40 reanalyses, and NCAR and NASA atmospheric model simulations. *J. Climate,* **18,** 1808–1830.

Schubert, S. D., M. J. Suarez, Y. Chang, and G. Branstator, 2001: Impact of ENSO on extratropical low frequency noise in seasonal forecasts. *J. Climate,* **14,** 2351–2365.

——, ——, P. J. Pegion, M. A. Kistler, and A. Kumer, 2002: Predictability of zonal means during boreal summer. *J. Climate,* **15,** 420–434.

——, ——, ——, R. D. Koster, and J. T. Bacmeister, 2004a: Causes of long-term drought in the U.S. Great Plains. *J. Climate,* **17,** 485–503.

——, ——, ——, ——, and ——, 2004b: On the cause of the 1930s dust bowl. *Science,* **303,** 1855–1859.

Seager, R., Y. Kushnir, C. Herweijer, N. Naik, and J. Velez, 2005: Modeling of tropical forcing of persistent droughts and pluvials over western North America: 1856–2000. *J. Climate,* **18,** 4065–4088.

Shuttleworth, W. J., 1991: Insight from large-scale observational studies of land/atmosphere interactions. *Surv. Geophys.,* **12,** 3–30.

Suarez, M. J., and L. L. Takacs, 1995: Documentation of the Aries/GEOS Dynamical Core: Version 2. NASA Tech. Memo. 104606, Vol. 5, 45 pp. [Available from Goddard Space Flight Center, Greenbelt, MD 20771.]

Ting, M., and H. Wang, 1997: Summertime U.S. precipitation variability and its relation to Pacific sea surface temperature. *J. Climate,* **10,** 1853–1873.

Trenberth, K. E., and C. J. Guillemot, 1996: Physical processes involved in the 1988 drought and 1993 floods in North America. *J. Climate,* **9,** 1288–1298.

Vose, R., R. Schmoyer, P. Steurer, T. Peterson, R. Heim, T. Karl, and J. Eischeid, 1992: The Global Historical Climatology Network: Long-term monthly temperature, precipitation, sea level pressure, and station pressure data. ORNL/CDIAC-53, NDP-041, Carbon Dioxide Information Analysis Center, 189 pp. [Available from Oak Ridge National Laboratory, Oak Ridge, TN 37831.]